

EVALUATION OF DIFFERENT ATMOSPHERIC CORRECTION ALGORITHMS FOR EO-1 HYPERION IMAGERY

B. T. San ^{a,*} and M. L. Suzen ^b

^a General Directorate of Mineral Research and Exploration (MTA), Remote Sensing Center, 06520, Ankara, Turkey – (tanersan@gmail.com.tr)

^b Middle East Technical University, Department of Geological Engineering, Remote Sensing and GIS Lab., 06531, Ankara, Turkey – (suzen@metu.edu.tr)

Commission VIII, WG VIII/3

KEY WORDS: Atmospheric Correction, Hyperion, ACORN, FLAASH, ATCOR2, ATCOR3

ABSTRACT:

Hyperspectral remote sensing is a powerful tool in discriminating lithological units and in preparation of mineral maps. Hyperion is a space borne sensor of Hyperspectral imagery having 220 channels within the 400 nm to 2500 nm wavelength range. Although the technical specifications of the sensor are quite high, in the operational stage there exist many nuisances like atmosphere. The presence of atmosphere with aerosols and gases alters the reflected signal from the surface resulting in a decrease in the quality of the Hyperion image. In order to obtain accurate and reliable results, atmospheric correction must be carried out for Hyperion data. There are many atmospheric correction algorithms based on MODTRAN or LOWTRAN in literature and/or in commercial use. In this study, the Atmospheric CORrection Now (ACORN), the Fast Line-of-sight Atmospheric Analysis of Spectral Hypercubes (FLAASH), and ATmospheric CORrection (ATCOR 2-3) atmospheric correction algorithms were tested for atmospheric correction of Hyperion data. Test site is located on Central Anatolia having sparse vegetation cover. Both the obtained resultant images and the whole spectral signatures from the field samples were compared with cross correlations of whole spectra and specific wavelengths in spectral domain. Despite the compromises in different wavelength regions ACORN is found to be a slightly better corrector algorithm for natural earth materials through lithological and mineralogical mapping needs.

1. INTRODUCTION

Hyperspectral images such as Hyperion are widely used for mineral mapping and lithological discrimination of the geological units (Kruse et. al., 2003, Rowan et. al., 2004, Hubbard and Crowley, 2005, van Ruitenbeek et. al., 2006, San, 2008). Narrow band widths with numerous channels possess much information about the investigation site surface. Even though, images have number of spectral channels, spectral images never depict the true radiance of the surface due to the sensors and atmosphere. (Adams and Gillespie, 2006) Therefore, if the image is atmospherically not corrected, none of the process results would be accurate. In order to avoid these kinds of problem, atmospheric correction or radiometric calibration should be performed before starting the classification processes.

This study presents results of the completed stages of an ongoing research about mineral mapping with Hyperion data. As a rule of thumb atmospheric correction is an indispensable step in the preprocessing of the Hyperspectral image analysis, however there are number of absolute atmospheric correction methods based on MODTRAN or LOWTRAN in literature. The purpose of the study is to compare different atmospheric correction techniques which are the Atmospheric CORrection Now (ACORN), the Fast Line-of-sight Atmospheric Analysis of Spectral Hypercubes (FLAASH), and ATmospheric CORrection (ATCOR 2-3) and to evaluate their successes from the scope of lithological mapping and mineral mapping.

2. STUDY AREA AND USED DATA

Study area is a narrow long strip of Hyperion image located on the central Anatolia having sparse vegetation cover. The study area located at on Kirsehir and Aksaray provinces of Turkey (Figure 1), having characteristic continental climate. The oldest rock unit in the area is a group of metamorphic rocks. Apart from these metamorphics, many different outcrops are present in the study area as Quaternary units, Miocene-Pliocene Volcanic Rocks, Miocene-Pliocene continental clastics and carbonates, Oligocene continental clastics, Upper Cretaceous-Paleocene Gabbro and granitoids (Figure 1) (Atabey, 1989).

Data used in the study are categorized into three groups which are hyperspectral data, the ASD field spectrometer measurements of 15 samples collected from the field, and ancillary data containing various geological maps prepared by General Directorate of Mineral Research and Exploration (MTA) and topographical base maps prepared by General Command of Mapping.

The major data source is EO1- Hyperion imagery acquired on November 17, 2002. Hyperion has 220 spectral channels having 30 m spatial resolution within 400 to 2500 nm wavelength range. 35 and 172 bands are located on the near infrared region and short wave infrared region, respectively. The swath width of the Hyperion is 7.5 km, where as characteristic scene size is 7.5 x 100 km, a narrow strip (Beck, 2003).

* Corresponding author.

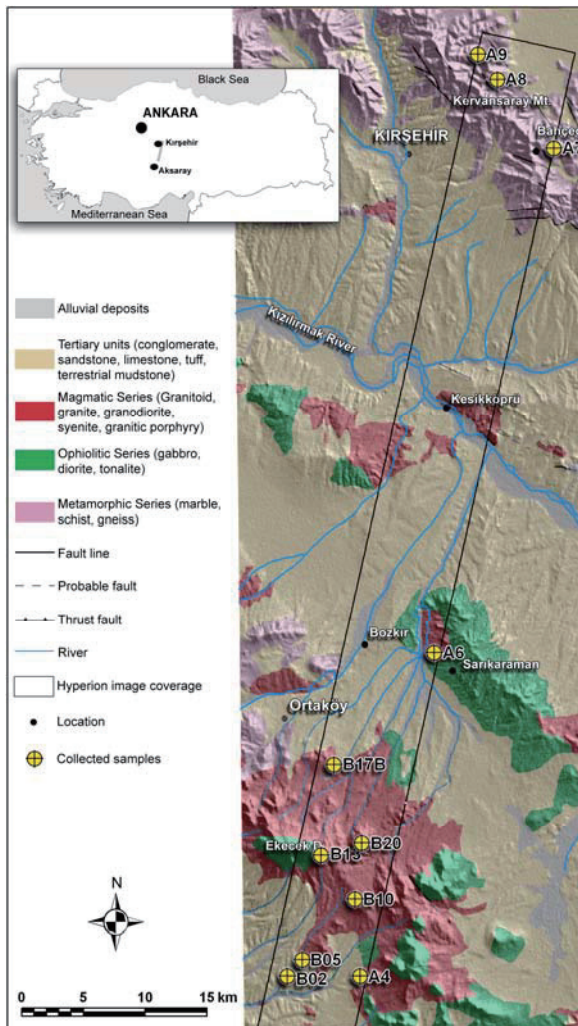


Figure 1: Location and simplified geological map of test site and collected samples.

3. BACKGROUND STUDIES

Passive remote sensing is based on interaction between light and material. Each mineral and rock unit has their own spectral responses where the working principle of imaging spectrometers is based on this statement. Therefore, if remotely sensed data has high spectral resolution with continuous wavelength range, the materials can be distinguished by using their spectral features (Okada and Iwashita, 1992). In addition, the narrower the band width, the higher the discrimination capacity of the sensor (Clark, 1999).

Even though Hyperspectral data have ability to distinguish surface materials especially in geology, agriculture and botany, there exists a need for preprocessing stages to get reliable and accurate results. Owing to the atmospheric gases and aerosols, atmospheric or radiometric corrections are required. Different gases in the atmosphere absorbs or transmit the light depend on the wavelength of the energy. Atmospheric correction of Hyperspectral data is therefore an obligation for radiance to reflectance conversion.

During the atmospheric correction, raw radiance data from imaging spectrometer is re-scaled to reflectance data. Therefore, all spectra are shifted to nearly the same albedo. The resultant spectra can be compared with the reflectance spectra of the laboratory or field spectra, directly.

Atmospheric correction techniques can be divided into two categories which are relative and absolute or empirical atmospheric corrections. The relative atmospheric correction can be divided into three sub-categories; flat field correction, internal average relative reflection correction, and empirical line correction. All the relative correction techniques utilize image data statistics such as average of the each band, minimum and maximum values of the bands with the target (mainly spectrally flat and homogeneous areas). In relative reflectance correction techniques, there is no need to a priori knowledge of the surface characteristics and atmospheric model option. Scattering and absorption of water vapor, mixed gases and topographic effects can be corrected using absolute reflectance methods. Radiative transfer codes (i.e. LOWTRAN and MODTRAN) can model the effects of scattering in the atmosphere. Using scattering and transmission properties of the atmosphere, the difference between the radiation leaving the earth and the radiation received at the sensor is modeled by radiative transfer codes having typical atmosphere models for a large number of atmosphere types for calculation of atmospheric radiance spectrum on a pixel-by-pixel basis. The surface reflectance is attained by the ratio of radiance at the sensor to the model solar irradiance.

Absolute atmospheric correction is more preferable than the relative correction techniques (Nikolakopoulos et. al., 2002) as, it models the atmosphere according to the similar environmental and geographical conditions when the image is acquired.

Atmospheric CORrection Now (ACORN) is stand-alone software which is developed for atmospheric correction of hyperspectral and multispectral imageries. ACORN is also based on MODTRAN 4 radiative transfer code, carried out a study for comparing the field spectra and atmospherically corrected Hyperion data in Yerington, Nevada. In their studies, not only ACORN, but also ATREM and HATCH-2d were used for atmospheric correction of AVIRIS image data. The study exemplified that except for 0.9 to 1.14 μm water vapor region, atmospheric correction models work well.

The Air Force Research Laboratory, Space Vehicles Directorate (AFRL/VS) develops a software package, the Fast Line-of-sight Atmospheric Analysis of Spectral Hypercubes (FLAASH) atmospheric correction code which derives its physics-based algorithm from the MODTRAN4 radiative transfer code (Felde et. al., 2003). FLAASH is designed to eliminate atmospheric effects caused by molecular and particulate scattering and absorption from the radiance at the sensor and to obtain reflectance at the surface. The Normalized Optical Depth Derivative (NODD) and atmospheric absorption features are used for an automated wavelength recalibration algorithm in FLAASH. Felde et. al., (2003) utilized Hyperion data to test the FLAASH in the Coleambally, Australia agricultural area, where their results showed that FLAASH is very useful tool for atmospheric correction.

ATCOR is used for computing a ground reflectance image for the reflective spectral bands, and emissivity images for the thermal bands. ATCOR algorithm has been developed in the last decade in two different types (ATCOR 2 and ATCOR 3) which are created by Dr. Richter of the German Aerospace Center - DLR. For nearly horizontal surface or flat terrain, ATCOR 2 is a spatially-adaptive fast atmospheric correction algorithm, whereas, ATCOR 3 is designed for rugged topographical surface, hence a Digital Elevation Model (DEM) is used in the ATCOR 3 algorithm for atmospheric correction.

In reality, earthly materials are found in a mixture which contains different minerals. There are four main types of mixtures which are aerial, intimate, coatings, and molecular mixtures (Clark, 1999). In aerial mixtures, there is no multiple scattering observed between components. If the different materials are in intimate contact in the scattering surface such as mineral grains in a rock unit, then the mixture is intimate mixture (Clark, 1999). Most of the hyperspectral studies on lithologic and mineralogical discrimination were carried out in ideal areas having nearly homogenous outcrops, less amount of atmospheric aerosols on desert area and minimal amount of vegetation cover such as Nevada, USA and Australia deserts (Okada and Iwashita, 1992, Kruse et. al., 2002, Kruse et. al., 2003, van Der Meer, 2004, Rowan et. al., 2004, van Ruitenbeek et. al., 2006). On the other hand, the test site of the study covers not only mono-mineralic outcrops but also some intimate mixtures like lithological units. In order to assess the different atmospheric correction techniques, this location is chosen as a test site.

4. METHODOLOGY

In this study four different atmospheric correction techniques are compared beyond the scope of two different aspects. One of them is the cross-correlation between spectrum of atmospherically corrected image pixel and field spectra measurements of this corresponding pixel carried out using ASD Field Spec II field spectrometer. The other aspect is the comparison of absorption features of spectral curves with the reference spectrum in specific wavelength regions. For both comparisons, 15 field sample spectra (A1, A2, A3, A4, A6, A7, A8, A9, B2, B5, B10, B12, B13, B17, and B20) are used as a reference data source for the test site (Figure 1).

In order to perform appropriate comparisons of the atmospherically corrected images, 15 representative sample locations were selected within the test site. A detailed sampling strategy is applied considering that all of the samples should be taken from uniform and largely outcropping rock units as much as it could be possible. 10 of the Samples (A2, A3, A4, A6, B2, B5, B10, B13, B17, and B20) are mainly from granitic rock units with differing mineralogies and differing alteration stages. Sample A1, A9, B12 are collected from reddish continental sandstone, schist, and gabbro units, respectively, whereas sample A7 and A8 are from marble (Figure 1). After that, all of the collected hand specimens are measured multiple times using ASD Field Spec II field spectrometer within 350 nm and 2500 nm range with a 1 nm band with (Figure 2).

Except for the ATCOR3 atmospheric correction technique, geometric correction process is performed at the end of atmospheric correction methods to keep original DN values of the imagery. ATCOR3 utilizes Digital Elevation Model (DEM) for atmospheric correction; hence, it is necessary to register the image data and DEM to a reference map.

At the beginning of the atmospheric correction applications, uncalibrated image channels of EO-1 Hyperion data are eliminated. Radiometrically calibrated channels are band numbers from 8 to 56 in VNIR and from 78 to 224 in SWIR regions electromagnetic spectrum (Beck, 2003). A Total of 49 and 147 bands are calibrated for VNIR and SWIR wavelength regions, respectively. The removed channels have either full of noise or having no data. After channel selection and removal stage, final Hyperion imagery has 196 spectral channels that would be used as input data for atmospheric correction algorithms.

In the first scheme ACORN 5.1 software is used. At the beginning of the computation, ASCII text files including individual channel wavelengths and corresponding Full Width Half Maximums (FWHM), gains and offset values are prepared. In addition, scene center coordinates, mean elevation, sensor altitude, image acquisition date and time are given as input parameters. Upon preparation of the text file and entering the related parameters, the software is run. ACORN software does not have any visualization module, and then the resultant image is displayed by using ENVI.

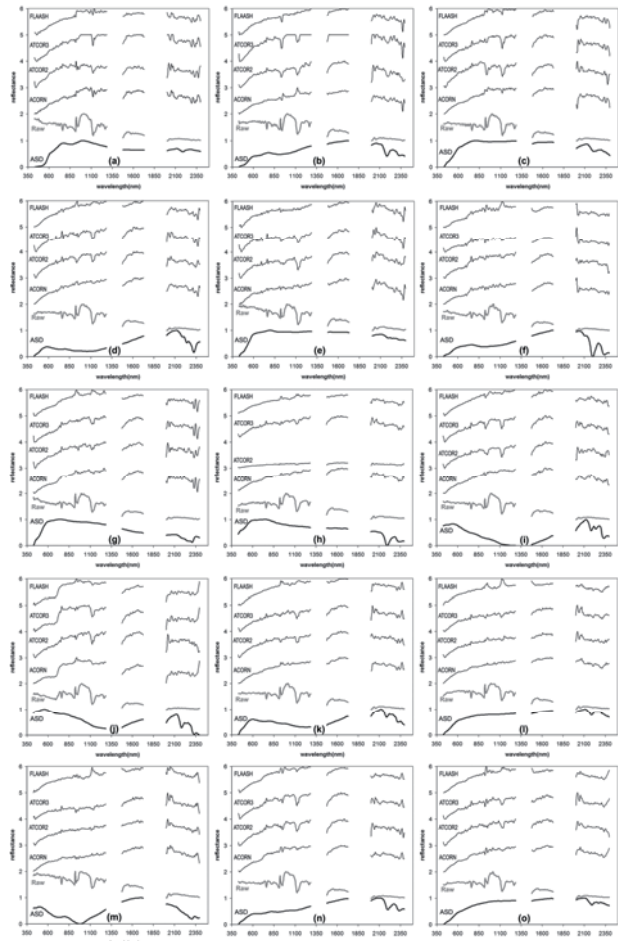


Figure 2. Spectral curve of the samples (A1, A2, A3, A4, A6, A7, A8, A9, B2, B5, B10, B12, B13, B17, B20 (from a to o)) for ASD field spectrometer as reference spectra, corresponding pixels of original data namely as Raw, ACORN, ATCOR2, ATCOR3, and FLAASH corrected spectra from bottom to top of each plot.

Next, the other atmospheric correction algorithm, FLAASH module of ENVI image processing software, is applied on the raw Hyperion image having 196 channels. At the beginning of this operation, Hyperion data is converted to BIL (Band Interleaved by Line) format. Similar to ACORN process, same parameters are entered as input.

The third atmospheric correction module, ATCOR2, works within the PCI Geomatica Image Processing software. The same image and the same conditional parameters (in ACORN and FLAASH) are entered as input for this operation.

The last atmospheric correction scheme to be applied is ATCOR3 which requires DEM data for correction. 1:25 000 scaled topographical vector maps having 10 m contour interval from General Command of Mapping, Turkey is used as source

for DEM generation. DEM generation by triangulation method and its accuracy is assessment is carried out using Erdas Imagine image processing and analysis software with 30 m grid size. In order to use ATCOR3 with Hyperion data, it should be coincided with DEM, hence raw Hyperion image is geocoded. The extent of the Hyperion imagery is a long rectangle having 100 km length and 12.7 degrees of azimuthal deviation in long axis. This long skinny extent yielded in uneven distribution of Ground Control Points (GCPs) where the polynomial models in ordinary rectification are not found to be suffice for geometric correction. In order to obtain a better fitted model, the image is orthorectified. The Hyperion image was orthorectified to Universal Transverse Mercator (UTM) projection using 12 GCPs with Erdas Imagine software for image. The residual errors were obtained as ± 0.419 and ± 0.868 pixels for easting and northing respectively, where the total root mean square error (RMSE) was ± 0.964 pixels.

After obtaining four atmospherically corrected images, spectral measurements are carried out in the field. The anomalous absorption bands attributed to water vapor are eliminated. The major water absorption features are located in 1400 and 1900 nm (Clark, 1999), eliminated 1340-1450 nm and 1750-1970 nm wavelength regions for water absorption. According to the spectra of atmospherically corrected images, corresponding channels located on 1296 to 1467 nm and 1740 to 1992 nm wavelength regions are ignored as sensor noise and water absorption regions.

Following the water absorption and sensor noise removal stage all atmospherically corrected and reference spectral curves of corresponding samples were normalized to range between 0 and 1 for competent two fold comparison.

In cross correlation comparison of the spectral curves of the atmospherically corrected images and reference data, it is seen that completely opposite trends could exist in the different wavelength regions. In order to achieve precise correlation coefficients, whole spectrum is divided into a number of different wavelength regions and is evaluated both separately, based on these newly formed regions and for whole spectra. The whole wavelength range between 426 nm and 2396 nm is divided into 3 sub-regions. The range between 426.82 nm and 1285.76 nm is defined as region 1, the range between 1477.43 nm and 1729.7 nm is described as region 2, and the range between 2002.06 nm and 2395.50 nm is identified as region 3. The correlation between reference field spectra and the atmospherically corrected image spectra reveal the overall similarity. On the other hand in geological hyperspectral remote sensing the pixels are generally intimately mixed hence the presence of individual marker mineral affects the whole spectra. In order to test the success of atmospheric correction algorithms another comparison scheme is implemented only considering the absorption features within specific wavelength regions.

5. RESULTS AND DISCUSSION

The two comparison schemes, cross correlation and comparison of absorption features in specific wavelengths, are used to evaluate the success of four different atmospheric correction methods. The following two sections give the obtained results and discussions to illustrate the differences or similarities in spectral domain.

5.1 The Results of the Cross Correlations between Image Data and Field Spectra Data for Each Atmospheric Correction Technique

The computed correlation coefficients (r) of the field samples are given in Table 1. The absolute value of correlation coefficient approaching to 1 indicates that the correlation is perfect and two data sets exactly fit to each other, whereas the sign of coefficient shows the direction of the relation. Conversely, if the correlation coefficient is nearly equal to zero, the two data sets are not correlated to each other. The minimum and the maximum correlation coefficients obtained through the analyses are as 0.00 and 0.97.

| | Full Region Correlation | | | | Region 1 Correlation | | | | Region 2 Correlation | | | | Region 3 Correlation | | | |
|--------|-------------------------|-----|-----|----|----------------------|-----|-----|----|----------------------|-----|-----|----|----------------------|-----|-----|----|
| sample | 426 – 2396 nm | | | | 426.82 – 1285.76 nm | | | | 1477.43 – 1729.7 nm | | | | 2002.06 – 2395.50 nm | | | |
| no | AC | AT2 | AT3 | FL | AC | AT2 | AT3 | FL | AC | AT2 | AT3 | FL | AC | AT2 | AT3 | FL |
| A1 | 65 | 75 | 60 | 68 | 82 | 91 | 84 | 83 | 64 | 52 | 59 | 61 | 0 | 5 | 0 | 0 |
| A2 | 74 | 73 | 67 | 76 | 87 | 90 | 83 | 92 | 80 | 66 | 29 | 80 | 49 | 42 | 48 | 47 |
| A3 | 70 | 75 | 67 | 70 | 75 | 83 | 75 | 75 | 87 | 93 | 93 | 83 | 24 | 34 | 29 | 21 |
| A4 | 7 | 4 | 6 | 3 | 1 | 3 | 3 | 1 | 82 | 66 | 67 | 84 | 42 | 41 | 37 | 39 |
| A6 | 51 | 40 | 44 | 55 | 78 | 74 | 72 | 80 | 69 | 35 | 45 | 68 | 64 | 66 | 70 | 61 |
| A7 | 35 | 29 | 33 | 26 | 72 | 70 | 69 | 66 | 87 | 77 | 83 | 65 | 19 | 22 | 19 | 15 |
| A8 | 16 | 8 | 11 | 15 | 38 | 45 | 37 | 36 | 85 | 80 | 82 | 87 | 6 | 6 | 5 | 6 |
| A9 | 0 | 0 | 1 | 1 | 0 | 1 | 2 | 0 | 34 | 19 | 18 | 45 | 49 | 17 | 57 | 47 |
| B2 | 54 | 33 | 43 | 55 | 91 | 73 | 79 | 90 | 76 | 68 | 64 | 74 | 39 | 21 | 29 | 38 |
| B5 | 13 | 16 | 12 | 17 | 54 | 57 | 47 | 55 | 86 | 78 | 81 | 86 | 4 | 23 | 3 | 5 |
| B10 | 8 | 14 | 11 | 5 | 0 | 1 | 0 | 0 | 81 | 66 | 69 | 78 | 39 | 52 | 29 | 29 |
| B12 | 87 | 85 | 81 | 75 | 93 | 92 | 93 | 86 | 84 | 72 | 73 | 5 | 19 | 20 | 13 | 5 |
| B13 | 20 | 14 | 28 | 14 | 34 | 38 | 26 | 33 | 91 | 88 | 90 | 19 | 68 | 66 | 54 | 66 |
| B17 | 37 | 45 | 40 | 34 | 86 | 86 | 82 | 86 | 84 | 70 | 72 | 82 | 20 | 29 | 25 | 15 |
| B20 | 89 | 85 | 85 | 83 | 97 | 95 | 93 | 95 | 80 | 65 | 75 | 8 | 21 | 44 | 20 | 11 |

Table 1. The correlation coefficient (%) of samples for full wavelength spectrum and regions of spectrum. The maximum values are underlined (AC: ACORN corrected image, AT2: ATCOR2 corrected image, AT3: ATCOR3 corrected image, FL: FLAASH corrected image).

The correlation values of each sample for whole spectrum is plotted and presented in Figure 3. As can be seen on this figure, sample A1, A2, A3, A6, B02, B12, and B20 have moderate to high correlations. On the contrary, samples A4, A7, A8, A9, B5, B10, B13, and B17 have low to moderate correlations with the reference. Especially, sample A9 has very low correlation values in whole spectrum and region 1. The sample is collected from schist and it has no obvious absorption features in the wavelength range between 350 nm and 2100 nm. Therefore, only distinction for the sample exists between the range of 2100 nm and 2360 nm. Similarly, sample A8 which is also schist has also low correlation coefficients. Rather than rock sample, another criterion for low correlation value is location of the image pixels corresponding to collected field samples. If the locations of the pixels are close to Hyperion image scene boundary such as sample A4, A6, A7, and A8, the existing noise around there is much higher than the scene center. The other factor for affecting the correlation success is presence of a potential mixture and unsampling of this mixture with the micro scale field sample compared to macro scale pixel on the image. On the other hand, shortwave infrared is required to discriminate most of the rock or soil. Therefore, region 2 and 3 are better for correlation of lithological units. In these regions, correlation coefficients also higher than the whole wavelength range comparison and region 1. Although some samples have low correlations, ACORN corrected samples have relatively high correlation comparing the corresponding competitor correction techniques on the same sample. Consequently, ACORN is found to be quite successful for atmospheric

correction of the Hyperion imagery according to the cross correlation results (San and Suzen, 2007).

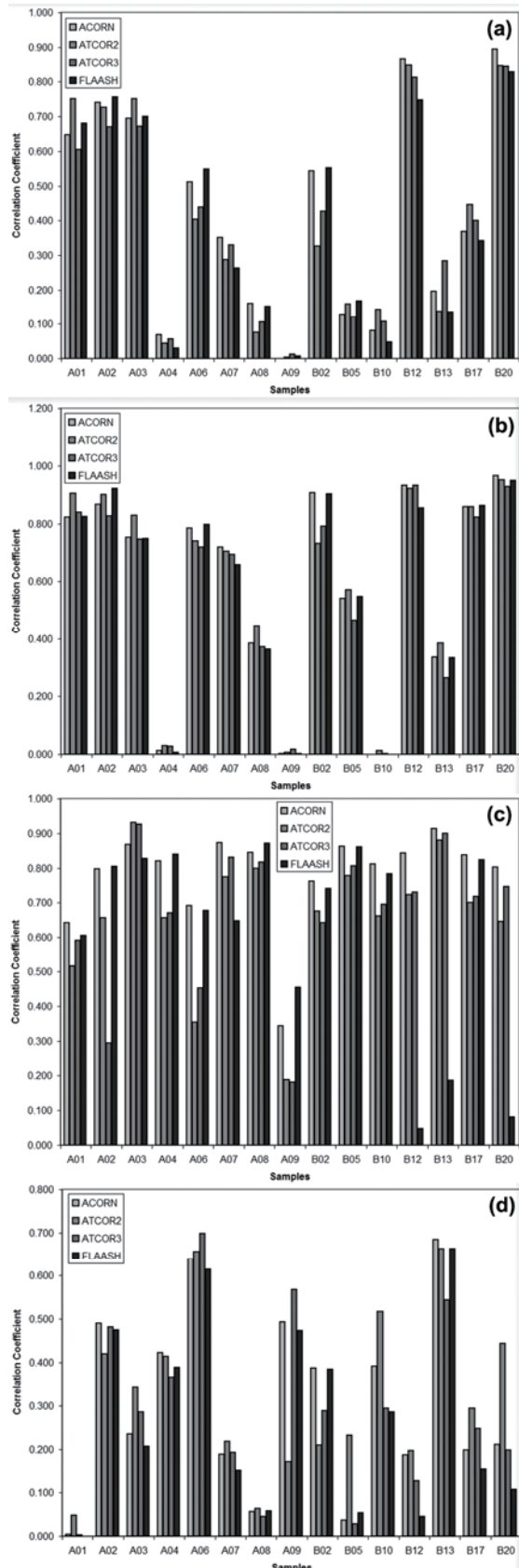


Figure 3. Correlations of each sample between reference spectra and atmospherically corrected images for full wavelength range (a), region 1 (b), region 2 (c), and region 3 (d).

5.2 The Results of the Comparison between Image Data and Field Spectra Data for Each Atmospheric Correction Technique Using Absorption wavelength

Although the atmospherically corrected image spectra of collected samples seem to be quite similar, there are some differences between reference spectra and the atmospherically corrected image spectra. The atmospheric correction technique is considered as successful, when a major absorption feature of reference spectra is coincided with the position of the absorption feature of atmospherically corrected one. For example, if the absorption wavelength of 2150.70 nm for Sample B2 is checked according to the reference spectrum, only ATCOR2 corrected data has consistency with the reference data. However, when the absorption wavelength of 2221.50 nm for B13 is compared with the ASD spectrum, all correction algorithms successfully detect this absorption feature (Figure 4). Table 2 summarizes the absorption wavelengths of the reference spectral samples and corresponding wavelength locations of four different atmospheric correction techniques. If the absorption wavelength position is in the correct location for the atmospheric correction, then it is marked as "1" otherwise marked as "0" on Table 2.

| Sample | Wavelength (nm) | ACORN | ATCOR2 | ATCOR3 | FLAASH |
|------------------|-----------------|--------------|--------------|--------------|--------------|
| A1 | 2150.70 | <i>1</i> | <i>1</i> | <i>1</i> | <i>1</i> |
| A2 | 2150.70 | <i>1</i> | <i>1</i> | <i>1</i> | <i>1</i> |
| A3 | 2158.50 | <i>1</i> | <i>1</i> | <i>1</i> | <i>1</i> |
| A4 | 2187.75 | 0 | 0 | 0 | 0 |
| | 1482.30 | 1 | 0 | 0 | 0 |
| | 2232.30 | 0 | 0 | 1 | 1 |
| A6 | 1482.30 | 1 | 0 | 0 | 1 |
| | 1600.00 | 1 | 0 | 0 | 1 |
| | 2150.70 | 1 | 0 | 1 | 1 |
| A7 | 2155.35 | 1 | 0 | 1 | 0 |
| | 2235.45 | 0 | 0 | 0 | 0 |
| A8 | 2224.65 | 1 | 0 | 1 | 1 |
| A9 | 2155.35 | 0 | 0 | 0 | 0 |
| | 2235.45 | 1 | 0 | 1 | 1 |
| B2 | 2150.70* | 0 | 1 | 0 | 0 |
| | 2187.75 | 1 | 0 | 1 | 1 |
| | 2235.45 | 1 | 0 | 0 | 0 |
| B5 | 2147.70 | 1 | 0 | 1 | 1 |
| B10 | 1482.30 | 1 | 0 | 0 | 1 |
| | 2152.50 | <i>1</i> | <i>1</i> | <i>1</i> | <i>1</i> |
| | 2186.10 | <i>1</i> | <i>1</i> | <i>1</i> | <i>1</i> |
| | 2230.80 | <i>1</i> | <i>1</i> | <i>1</i> | <i>1</i> |
| B12 | 1482.30 | 1 | 0 | 0 | 0 |
| | 2152.50 | 0 | 0 | 0 | 0 |
| B13 | 1700.00 | <i>1</i> | <i>1</i> | <i>1</i> | <i>1</i> |
| | 2221.50* | <i>1</i> | <i>1</i> | <i>1</i> | <i>1</i> |
| | 2239.99 | 1 | 0 | 0 | 0 |
| | 1439.70 | 1 | 0 | 0 | 0 |
| | 1652.35 | <i>1</i> | <i>1</i> | <i>1</i> | <i>1</i> |
| B17 | 2160.00 | 1 | 1 | 0 | 0 |
| | 2240.00 | 1 | 0 | 1 | 1 |
| B20 | 1482.30 | 1 | 0 | 0 | 0 |
| | 1652.50 | <i>1</i> | <i>1</i> | <i>1</i> | <i>1</i> |
| | 2152.50 | 0 | 0 | 1 | 0 |
| | 2201.65 | 1 | 0 | 1 | 1 |
| Total (%) | | 28 | 12 | 20 | 21 |
| | | 75.68 | 32.43 | 54.05 | 56.76 |

Table 2. The main absorption wavelength of the reference spectra and the comparison of the corresponding region of atmospherically corrected image spectra. Italic characters (1) shows all the correction techniques are correctly detected and the bold characters (0) shows none of the atmospheric correction techniques detected the absorption feature.

According to the absorption features of the reference spectra, all the atmospheric correction algorithms clearly distinguish absorptions of the samples A1, A2, A3, and some absorption features of samples B10, B13, B20. On the contrary, some of

the absorption wavelengths of samples A4, A7, A9, and B12 cannot be identified correctly as an absorption by the atmospheric correction algorithms. As a result of the comparison, ACORN can detect the 28 absorption features correctly out of total 35 absorption features on 15 different samples. FLAASH, ATCOR3, and ATCOR2 can detect only 21, 20, and 12 absorption features with corresponding wavelength given in Table 2, respectively.

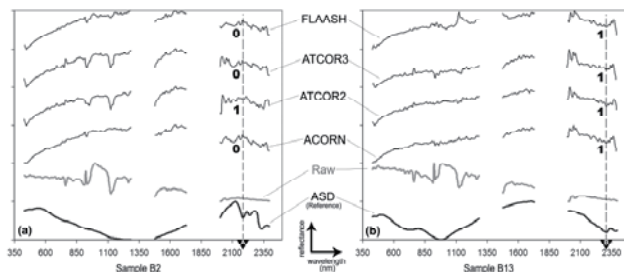


Figure 4. Example of absorption feature comparison for sample B2 (a) and sample B13 (b). Vertical lines A and B stands for wavelengths of 2150.70 nm and 2221.50 nm.

6. CONCLUSIONS

During the study, it is proposed to compare and evaluate the success of the four different atmospheric corrections for Hyperion data beyond the scope of lithological and mineralogical mapping. All algorithms are compared with two different approaches; one with regional-spectral correlations with the reference data and the other with individual absorption features. As a result of the study, all the atmospheric correction methods applied on the data are found to be successful in overall evaluation but with compromises varying in different wavelength regions. Despite the compromises in different wavelength regions ACORN is found to be a better corrector algorithm for natural earth materials through lithological and mineralogical mapping needs.

7. ACKNOWLEDGEMENTS

The authors would like to thank Assoc. Prof. Dr. Nuretdin Kaymakci (RS-GIS Lab. Dept. of Geol. Eng., METU-Ankara/Turkey) for his valuable comments. The authors also would like to express their sincere gratitude to Murat Koruyucu (Remote Sensing Center, MTA - Ankara) for his company in field studies in addition to his suggestions about the manuscript.

8. REFERENCES

- Adams, J. B. and Gillespie, A. R., 2006. *Remote Sensing of Landscapes with Spectral Images: A Physical Modeling Approach*. Cambridge University Press, p 362.
- Atabay, E., 1989. *1:100 000 ölçekli Açınsama Nitelikli Türkiye Jeoloji Haritaları Serisi, Aksaray – H 18 Paftası*, Maden Tectik ve Arama Genel Müdürlüğü, Jeoloji Etütleri Dairesi, Ankara.
- Beck, R., 2003. *EO-1 User Guide*, Version 2.3., 74 p., University of Cincinnati.
- Clark, R. N., 1999. Chapter 1: Spectroscopy of Rock and Minerals, and Principles of Spectroscopy (chapter 1), *Remote Sensing for Earth Sciences: Manual of Remote Sensing*, 3.ed., Vol. 3, John Wiley and Sons, New York, edited by Andrew N. Rencz, pp. 3 – 58.
- Felde, G. W., Anderson, G. P., Cooley, T. W., Matthew, M. W., Adler-Golden, S. M., Berk, A., and Lee, J., 2003. Analysis of Hyperion Data with the FLAASH Atmospheric Correction Algorithm, *IEEE Transactions on Geoscience and Remote Sensing*, pp. 90 – 92.
- Hubbard, B. and Crowley, J. K., 2005. Mineral mapping on the Chilean–Bolivian Altiplano using co-orbital ALI, ASTER and Hyperion imagery: Data dimensionality issues and solutions, *Remote Sensing of Environment*, 99 (1-2), pp. 173-186.
- Kruse F. A., Boardman, J. W., and Huntington, J. F., 2002. Comparison of EO-1 Hyperion and Airborne Hyperspectral Remote Sensing Data for Geologic Applications. *IEEE Aerospace Conference Proceedings, IEEE Publication*, 3, pp. 3-1501 – 3-1513.
- Kruse F. A., Boardman, J. W., and Huntington, J. F., 2003. Comparison of Airborne Hyperspectral Data and EO-1 Hyperion for Mineral Mapping. *IEEE Aerospace Conference Proceedings, IEEE Transactions on Geoscience and Remote Sensing*, 41(6), pp. 1388 – 1400.
- Nikolakopoulos, K.G.; Vaiopoulos, D.A.; Skianis, G.A., 2002. A Comparative Study of Different Atmospheric Correction Algorithms Over An Area With Complex Geomorphology in Western Peloponnese, Greece, *Geoscience and Remote Sensing Symposium, IGARSS '02, IEEE International*, 4, pp. 2492 – 2494.
- Okada, K., & A. Iwashita, 1992. Hyper-multispectral Image Analysis Based on Waveform Characteristics of Spectral Curve. *Advances in Space Research*. 12: pp. 433–442.
- Rowan, L. C., Simpson, C. J., and Mars J. C., 2004. Hyperspectral Analysis of The Ultramafic Complex and Adjacent Lithologies at Mordor, NT, Australia. *Remote Sensing of Environment*, 91, pp. 419 – 431.
- San, B. T. and Suzen, M. L., 2007. Comparison of Atmospheric Correction Techniques for Hyperion Data, *ISPRS COMMISSION VII, WG2 & WG7, Conference on Information Extraction from SAR and Optical Data, with Emphasis on Developing Countries, Technical Session II: Optical Remote Sensing: High Resolution and Hyperspectral*, 16 - 18 May 2007, ITU, Istanbul.
- San, B. T., 2008. Hyperspectral Image Processing of Eo-1 Hyperion Data for Lithological and Mineralogical Mapping, *PhD. Thesis, METU, Department of Geological Engineering*, 142p.
- Van Der Meer, F., 2004. Analysis of spectral absorption features in hyperspectral imagery. *International Journal of Applied Earth Observation and Geoinformation*, 5, pp. 55 – 68.
- Van Ruitenbeek, F. J. A., Debba, P. Van Der Meer, F. D., Cudahy, T., Van Der Meijde, M., and Hale, M., 2006. Mapping White Micas and Their Absorption Wavelengths Using Hyperspectral Band Ratios, *Remote Sensing of Environment*, No. 102, pp. 211 – 222.